



Carbon nanotubes as a unique agent to fabricate nanoceramic/metal composite powders for additive manufacturing



Weiwei Zhou^a, Xiaohao Sun^a, Keiko Kikuchi^a, Naoyuki Nomura^{a,*}, Kyosuke Yoshimi^b, Akira Kawasaki^a

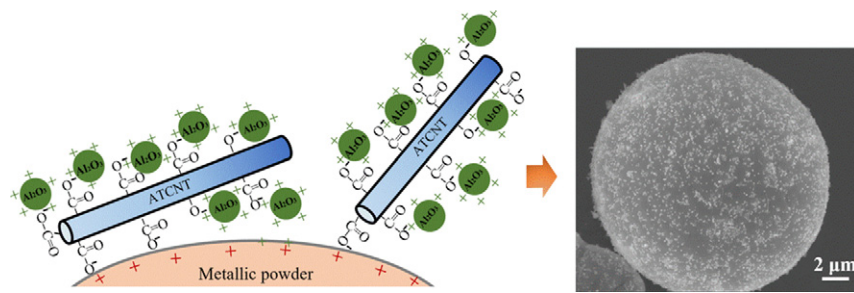
^a Department of Materials Processing, Graduate School of Engineering, Tohoku University, Sendai 980-8579, Japan

^b Department of Material Science, Graduate School of Engineering, Tohoku University, Sendai, Miyagi 980-8579, Japan

HIGHLIGHTS

- A novel application of CNTs was exploited for preparing nanoceramic/metal powders.
- The composite powders kept similar in shape, particle size, and distribution to raw metallic ones.
- The Al₂O₃-coated metallic powders showed higher laser absorptivity than uncoated ones.
- Al₂O₃ particles were uniformly dispersed and intimately contacted with the matrix after PBF.

GRAPHICAL ABSTRACT



ARTICLE INFO

Article history:

Received 31 July 2017

Received in revised form 1 October 2017

Accepted 12 October 2017

Available online 14 October 2017

Keywords:

Laser powder bed fusion

Metal matrix composites (MMCs)

Carbon nanotubes

Dispersion

Laser absorptivity

ABSTRACT

Laser powder bed fusion (PBF) offers many technological opportunities for producing high-performance composite parts with tailored structures. However, fabrication of suitable composite powders possessing homogeneous dispersion, good flowability, suitable particle size and distribution is a prerequisite and main challenge currently faced. In this study, a novel strategy was developed to prepare nanoceramic/metal powders by using acid-treated carbon nanotubes (ATCNTs) as an agent. In detail, a 3 wt% ATCNT/Al₂O₃ colloid, in which the negatively-charged ATCNTs were partially covered with positively-charged Al₂O₃ nanoparticles under electrostatic attraction, was obtained by heteroagglomeration; subsequently, the uncovered surface areas of ATCNTs were intimately bonded to the positively-charged MoTiAl powders during their mixing. This ATCNT bridging made individual Al₂O₃ uniformly wrap on the surface of MoTiAl without aggregation. The Al₂O₃-coated MoTiAl powders remained similar in shape, particle size, and distribution to uncoated ones, simultaneously showing higher laser absorptivity due to an increased surface roughness. The PBF-processed Al₂O₃-ATCNT/MoTiAl composite was dense, in which Al₂O₃ nanoparticles were homogeneously dispersed and intimately contacted with MoTiAl, giving rise to an increase in the hardness of the matrix.

© 2017 Elsevier Ltd. All rights reserved.

1. Introduction

Owing to their high specific strength, sufficient stiffness and excellent wear resistance, metal matrix composites (MMCs) have received increasing attention in many applications including aircraft, automotive

and energy storage [1,2]. In processing of MMCs, it is critical that the reinforcements are homogeneously dispersed and intimately incorporated into the matrix, which plays a vital role in determining the composite properties [3]. Currently, several manufacturing techniques such as casting [4], powder metallurgy [5,6] and mechanical alloying [7,8] are employed to produce MMCs. However, there are some existing problems, e.g., the insufficient densification rate and the irregular microstructure and aggregation of reinforcements, as well as the poor

* Corresponding author.

E-mail address: nnomura@material.tohoku.ac.jp (N. Nomura).

wettability and interfacial bonding between the reinforcements and the matrix, giving rise to resultant micro-cracks and even premature failure under loading [9,10]. In the meanwhile, the traditional methods usually involve highly time-, energy- and material-consuming processing steps [11]. Laser powder bed fusion (PBF), as a newly developed additive manufacturing technology, is capable of fabricating three-dimensional components directly by selectively melting raw powders using computer-designed CAD models [12–14]. Compared with traditional techniques, laser PBF provides many advantages, such as the direct production of complex structures, high material utilization rate, and high processing flexibility [14]. Furthermore, due to its non-equilibrium, rapid melting and solidification processing characteristics, laser PBF is expected to enhance the reinforcement/metal interfacial bonding [15]. Therefore, laser PBF offers new technological opportunities for producing high-performance MMC parts with tailored structures. Up till now, however, limited number of MMCs including TiC/TiAl [16], SiC/Fe [17], TiC/Al [18], TiB₂/Al [19], TiB₂/Inconel [20], Al₂O₃/Al [21,22], TiC/Ti [23], WC/Inconel [10], TiB₂/Ti [24], SiC/Al [25], TiB/Ti [26], TiB₂/TiAl [27], TiC/steel [28], Al₂Si₄O₁₀/Al [29] and Al₂O₃/Ni [30] by PBF have been reported.

The ever-increasing demand for novel heat-resistant materials beyond the realm of Ni-based superalloys has generated significant research interest in refractory intermetallics [31,32]. Mo-based alloys, possessing high melting points and high stiffness, are considered as promising candidates [32–34]. However, the unsatisfied elevated-temperature strength and poor processability of Mo-based alloys have seriously limited their application reliability [32,35]. It is well recognized that the mechanical strength of metals can be enhanced via the incorporation of uniform nanoceramic particles acting as a dislocation barrier [33]. Due to its low density, high hardness, high thermal stability, and excellent high-temperature creep resistance [36], the reinforcement of Al₂O₃ nanoparticle is widely used. For instance, Chen et al. [6] reported that Al₂O₃ dispersions could remarkably improve the elevated-temperature strength and fracture toughness of hot-pressed Mo₅Si₃. Therefore, PBF-processed Al₂O₃/Mo-based components with customized structures and enhanced performance have enormous potential for elevated-temperature service. Unfortunately, research regarding Mo-based alloys and their related composites by PBF, to the best of our knowledge, has rarely been documented.

It is known that the preparation of suitable powders is a prerequisite, but the main challenge currently faced is to broaden PBF in MMCs [14, 37]. The powders used for laser PBF should possess good flowability, suitable powder size (usually smaller than the diameter of a laser spot to be adequately melted), and narrow particle size distribution [38]. The previous studies [10,11,14–21,23,24] mainly focused on the morphologies and mechanical properties changed by reinforcements, while the influence of powder preparation on the PBF processability and final quality of MMCs was often ignored. In most works (see Table 1), the mixed powders were prepared by low-energy blending (LEB) and high-energy ball milling (HEBM). LEB is known for its feasibility of mixing two similarly micro-sized particles, while it is greatly limited for nanoceramic dispersion because nanoparticles are easily agglomerated when driven by strong van der Waals forces due to their high aspect ratio. In contrast, HEBM is capable of breaking tangled nanoparticles and dispersing nanoparticles into the matrix. However, HEBM involves uncertainty in tailoring the metallic powder size and distribution [11]. More importantly, severe plastic deformation usually occurs in HEBM-processed metallic powders, thus they tend to be flaky in the spherical shape or to be tangled with cold welding [16], showing poor flowability. Based on the above, it is imperative to develop a novel process that not only addresses the dispersion issue of nanoceramics but also keeps the features of the original metallic powders (e.g., shape, particle size, and distribution). This task is a dominating step for PBF.

The heteroagglomeration method is deemed to be an effective approach for mixing powders, such as in Al₂O₃/protein [39], SiO₂/polymer [40], and nano carbon/ceramic systems [41]. This method is based on the principle of electrostatic attraction that generally applies to two

Table 1
Characteristics of different methods in powder preparation for laser PBF.

Methods of powder preparation	Authors	PBF-processed MMCs	Starting powders and particle size	Advantages	Disadvantages			
Low-energy blending (LEB)	Rong et al. [10,15]	WC _{1-x} /Inconel	WC _{1-x} : 15–45 μm, Inconel 718: 25–45 μm	Fast and easy; nearly keep the shape, particle size, and distribution of metallic powders; good powder flowability	Limited for similarly micro-sized particles; poor dispersion for nano-sized reinforcements			
	Li et al. [25]	SiC/Al ₁₂ Si	SiC: 11–45 μm, Al ₁₂ Si: 20–63 μm					
	Attar et al. [26]	TiB/Ti	No information provided					
	Zhang et al. [20]	TiB ₂ /Inconel	TiB ₂ : 11–45 μm, Inconel 718: 5–12 μm					
	Han et al. [21]	Al ₂ O ₃ /Al	Al ₂ O ₃ : 10 nm, Al: 17 μm					
	Jue et al. [22]	Al ₂ O ₃ /Al	Al ₂ O ₃ : 9 μm, Al: 1 μm					
	Gu et al. [23]	TiC/Ti	TiC: 50 nm, Ti: 23 μm					
	Gu et al. [18]	TiC/AlSiMg	TiC: 50 nm, AlSi ₁₀ Mg: 30 μm					
	Song et al. [17]	SiC/Fe	SiC: 27 μm, Fe: 20 μm					
	Li et al. [27]	TiB ₂ /TiAl	TiB ₂ : 3–5 μm, TiAl: 28 μm					
High-energy ball milling (HEBM)	AlMangour et al. [28]	TiC/steel	TiC: 50 nm or 1 μm, Stainless steel: 45 μm	Fast and easy; good dispersion of reinforcements	Involving uncertainty in tailoring the metallic powder size and distribution; metallic powder shape changed; poor powder flowability; including undesirable phases or contamination			
	He et al. [37]	TiC/Ti	TiC: 45 nm, Ti: 25 μm					
	Attar et al. [24]	TiB/Ti	TiB ₂ : 3.5–6 μm, Ti: 49 μm					
	Jue et al. [29]	Al ₂ Si ₄ O ₁₀ /Al	Al ₂ O ₃ : 9 μm, AlSi ₁₀ Mg: 30 μm					
	Gu et al. [16]	TiC/TiAl	Ti: 30 μm, Al: 16 μm, graphite: 30 μm					
	Ma et al. [30]	Al ₂ O ₃ /Ni, SiC/Ni	Ni, Al ₂ O ₃ : 50 nm, SiC: 50 nm					
	Li et al. [19]	TiB ₂ /AlSiMg	nano-TiB ₂ , Al–Si alloy, pure Mg					
	Electro-codeposition Melting + gas-atomization						Good dispersion of reinforcements Good dispersion; spherical powder shape; good flowability; controllable size and distribution	Complex; costly, limited powder quantity Complex; costly; difficult for refractory alloys

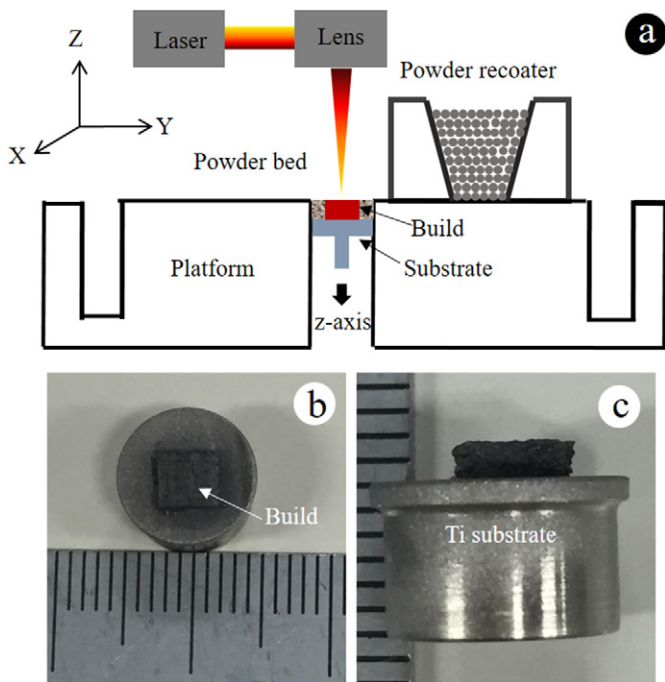


Fig. 1. (a) The typical layout of in-house developed laser PBF machine; (b) the top view and (c) side view of a typically PBF-processed 5%Al₂O₃-0.15%ATCNT/MoTiAl build.

oppositely charged colloidal species [41]. For oxide ceramic or metallic powders (usually containing some oxide structures on their surface) after dispersing into the water or ethanol, H⁺ ions are preferentially adsorbed on the particle surface so that the powders are positively

charged [5,41]. This means that an electrostatic attraction between the Al₂O₃ nanoparticle and Mo-based powder hardly occurs because they have the same surface charge. To address this issue, our idea is to introduce a negatively charged agent to bridge positively charged Al₂O₃ and Mo-based powders during heteroagglomeration. This process should be surfactant-free to avoid residual contamination in composite powders.

Recently, carbon nanotubes (CNTs) have attracted great attention for strengthening MMCs due to their low density (2.1 g cm⁻³), high tensile strength (~100 GPa), high Young's modulus (~1 TPa), and excellent thermal/electrical conductivities [42]. Since pristine CNTs are prone to being easily tangled, acid treatment is widely employed to modify their surfaces [43]. The surface of acid-treated CNTs (ATCNTs) is coated with an abundance of hydrophilic groups; this results in ATCNTs being negatively charged and stably suspended in solvent [43]. Moreover, ATCNTs could remain remarkably stable thermally with intrinsic strength as reinforcements, even though certain disorders are present on their outer walls [5]. In this regard, ATCNTs are supposed to be an agent suitable for bridging two positively charged species. In this work, therefore, a novel strategy using ATCNT agents without a surfactant was put forward to fabricate Al₂O₃/metal powders for PBF. The role of ATCNTs in powder mixing was clarified based on careful observations of the Al₂O₃ dispersion and the existential state of ATCNTs. The morphology of the PBF-processed Al₂O₃-ATCNT/metal composite, as well as the laser absorptivity of mixed powders, was also analyzed to verify the success of our strategy.

2. Experimental

2.1. Materials

A simple solid solution of Mo-33mass.%Ti-13mass.%Al system [44] was taken as one example of Mo-based alloys in this work. Unless

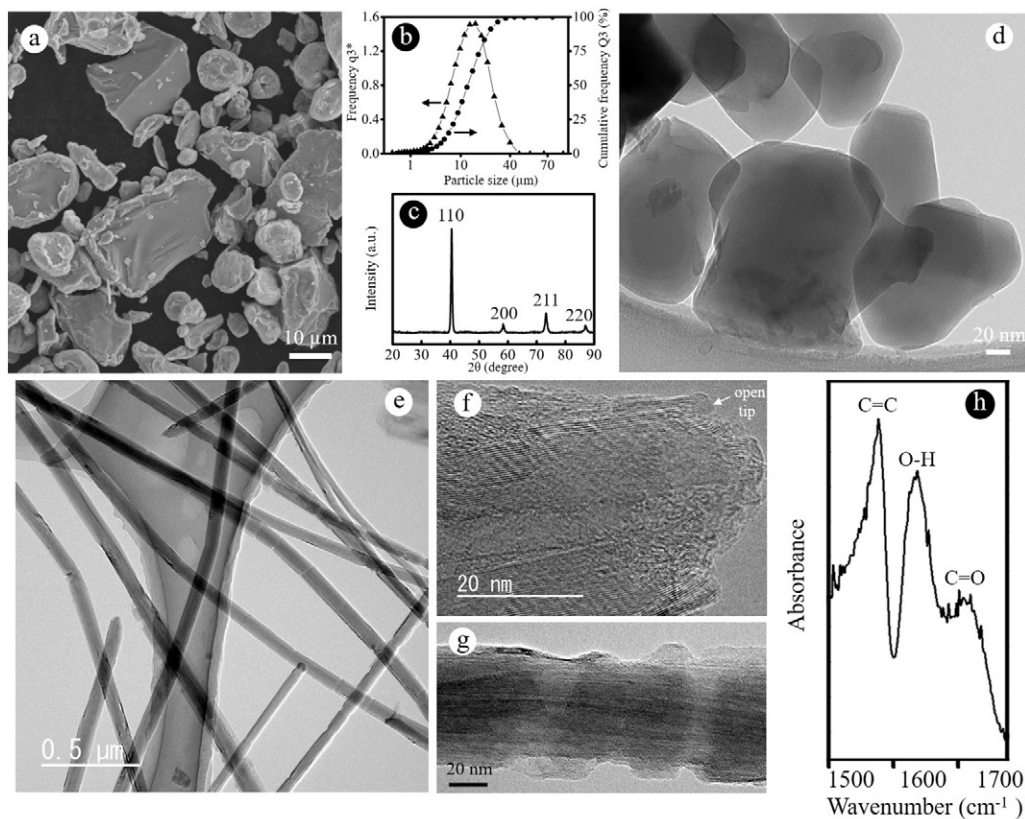


Fig. 2. (a) FESEM image and (b) particle size distribution and (c) X-ray diffraction pattern of raw MoTiAl powders; (d) TEM image of Al₂O₃ nanoparticles on a copper grid; (e–g) TEM images and (h) FTIR spectroscopy of ATCNTs.

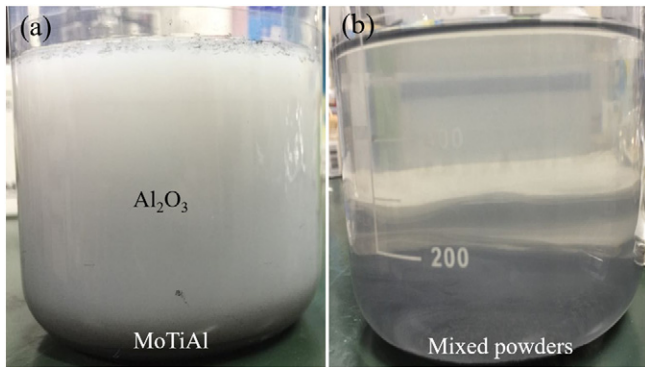


Fig. 3. Photographs of (a) the 10%Al₂O₃/MoTiAl and (b) 10%Al₂O₃-0.31%ATCNT/MoTiAl mixed colloids after settling for 2 h and 0.15 h, respectively.

otherwise mentioned, the compositions appear in mass percents. The MoTiAl powders were fabricated via conventional arc melting followed by mechanical milling and sieving. Commercially available Al₂O₃ nanoparticles having a purity of 99.9% were provided by Taimei Chemicals Co., Ltd., Japan. The pristine CNTs with a diameter of 20–110 nm and length of 2–15 nm were obtained from Hodogaya Chemical Co. Ltd., Japan. As reported elsewhere [43], the ATCNTs were prepared in an

ultrasonicated acidic mixture of 61% HNO₃ and 97% H₂SO₄ (1:3, v/v) at 323 K for 4 h. The HNO₃, H₂SO₄ and high-purity ethanol were provided by Wako Industries, Japan.

2.2. Fabrication of mixed powders

Firstly, appropriate amounts of ATCNTs, Al₂O₃, and MoTiAl powders were separately suspended in ethanol under ultrasonication in a water bath equipped with a mechanical stirrer for 2 h. The ATCNT suspension was then added drop by drop into an Al₂O₃ colloid to form a 3% ATCNT/Al₂O₃ hybrid. Subsequently, this ATCNT/Al₂O₃ hybrid was slowly incorporated into desired amounts of MoTiAl colloid, followed by mechanical stirring for 0.5 h. Finally, the composite powders of 5%Al₂O₃-0.15%ATCNT/MoTiAl, 10%Al₂O₃-0.31%ATCNT/MoTiAl, and 15%Al₂O₃-0.46%ATCNT/MoTiAl were obtained after completely drying in a vacuum at 353 K. For comparison, MoTiAl-10%Al₂O₃ and MoTiAl-0.31%ATCNT mixed powders were also prepared by heteroagglomeration.

2.3. Laser PBF process

All bulk samples were produced on an in-house developed laser PBF machine, as shown in Fig. 1a. This machine is equipped with a Yb: YAG fiber laser source (Raycus Fiber Laser Technologies Co., Ltd., Wuhan), which produces a laser beam with a wavelength of 1070 nm and a

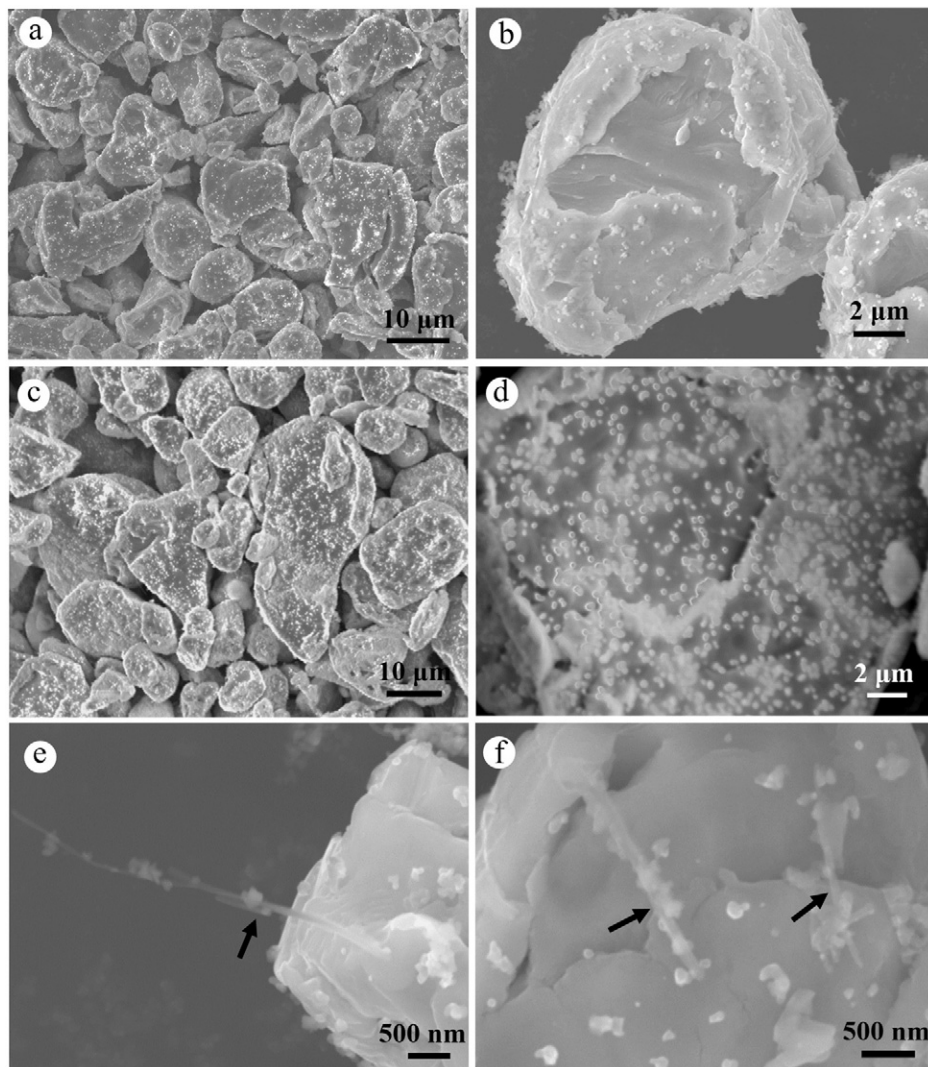


Fig. 4. FESEM images of (a, b) 5%Al₂O₃-0.15%ATCNT/MoTiAl and (c, d) 10%Al₂O₃-0.31%ATCNT/MoTiAl composite powders; (e, f) typical examples of individual ATCNTs (see black arrows) bridging the Al₂O₃ and MoTiAl powders.

Table 2

D_{10} , D_{50} and D_{90} values for particle size distribution of raw MoTiAl and Al_2O_3 -ATCNT/MoTiAl composite powders.

	D_{10} (μm)	D_{50} (μm)	D_{90} (μm)
MoTiAl	5.10	12.81	24.93
5% Al_2O_3 -0.15%ATCNT/MoTiAl	5.22	13.02	25.48
10% Al_2O_3 -0.31%ATCNT/MoTiAl	4.99	13.15	25.69

maximum power of 22 W in continuous mode. The laser has the fundamental transverse Gaussian mode (TEM_{00}) and the spot diameter of 45 μm . A set of optimized laser PBF parameters (laser power: 20.6 W, scanning speed: 10 mm s^{-1} , hatch distance: 100 μm , layer thickness: 25 μm) and typical “X–Y alternately scanning strategy” [14] were utilized for fabricating both raw MoTiAl and Al_2O_3 -ATCNT/MoTiAl composites in this work. The Ti substrates were preheated at 343 K. The building process was conducted under protective Ar atmosphere with a low oxygen content less than 0.1%. Rectangular samples with a width, length, and height of 4, 4, and 1.4 mm, as shown in Fig. 1b and c, were used for the microstructural and mechanical characterizations. Furthermore, in order to further prove the ability of laser PBF to deliver three-dimensional bulks, other three 5% Al_2O_3 -0.15%ATCNT/MoTiAl builds with different geometries were also fabricated (Fig. S1, Supporting information).

2.4. Characterizations

The microstructures of powders and PBF-processed bulks were evaluated by field-emission scanning electron microscope (FESEM; JSM-6500F, JEOL, Japan) and high-resolution transmission electron microscope (HRTEM; HF-2000EDX, Hitachi, Japan). For FESEM observations, the transversal and longitudinal cross-sections of bulks were successively grinded by SiC grinding papers (Struers Ltd.) with the grit numbers of 220, 500, 1000, 1500, 2000 and 4000, and then finely polished with the OP-S suspension (Struers Ltd.) consisting of colloidal silica and distilled water for 0.05 h. The TEM samples were prepared by grinding to the thickness of 50 μm , and thinned by the ion milling method (GATAN PISP Model 691, Gatan Inc.). The element distribution in Al_2O_3 -ATCNT/MoTiAl composite was performed by electron probe micro-analysis (EPMA) (JEOL JXA-8530F) and JEOL JEM-ARM200F electron microscope. The particle size distribution of powders was evaluated by a helium neon laser optical system (HELOS H1051, SHIMADZU, Japan). The X-ray diffraction (XRD) patterns were collected by Rigaku Smartlab 9 kW diffractometer. Functional groups in ATCNTs were checked using a Fourier transform spectrometer (FTIR 6300, JASCO, Japan) in a wavenumber range of 1500–1800 cm^{-1} . The zeta potential was measured using a zeta meter (Malvern Instruments, Ltd., UK) in ethanol. Before the measurements, all powders were ultrasonicated for 1 h to achieve a homogeneous dispersion. The laser absorptivity testing was conducted with a V-670 UV-VIS-NIR spectrophotometer (JASCO, Japan). Micro-Raman spectra were measured with a SOLAR TII Nanofinder (Tokyo instruments Co.) with 532 nm wavelength incident laser light. The Vickers hardnesses of the polished bulks were measured

by using a FISCHERSCOPE HM200 microhardness tester (FISCHER, Germany), according to ISO standard 14,577-1:2015. The indenter was continuously loaded to the peak load of 0.588 N in 60 s and unloaded after a holding time of 30 s to allow a full plastic deformation. At least ten locations were measured for each sample, and then the values were averaged.

3. Results and discussion

Characterizations of raw MoTiAl, Al_2O_3 and ATCNTs powders were displayed in Fig. 2. The XRD pattern reveals that the MoTiAl exhibited characteristic reflections of body-centered cubic structure (Fig. 2c). Raw MoTiAl powders are irregularly shaped (Fig. 2a), and their particle sizes are in a range of 1–45 μm with a mean value of 12.8 μm (Fig. 2b). Even though this irregular shape may influence the flowability of MoTiAl powders, it was demonstrated that a dense MoTiAl build could be obtained by PBF processing in this work. Al_2O_3 nanoparticles possessed a near-spherical shape with an average diameter of 140 nm (Fig. 2d). This large size difference makes difficult to achieve homogeneous dispersion of Al_2O_3 among MoTiAl powders. According to zeta potential measurements, the Al_2O_3 was strongly positively charged in ethanol (~ 29.3 mV), while the surface of MoTiAl carried a weak positive charge (Fig. S2, Supporting information).

The ATCNTs were straight and slender, displaying a high aspect ratio (Fig. 2e). High-resolution TEM (HRTEM) images revealed that the ATCNTs had an open-end structure (Fig. 2f), and some nanodefects were induced on their outer walls (Fig. 2g). These nanodefects and open tips contain the dangling bonds of carbon atoms, showing a higher chemical activity. In FTIR spectroscopy of ATCNTs (Fig. 2h), the primary peaks involve the C=C vibration model at 1580 cm^{-1} in graphene sheets and the O–H stretching vibration at 1634 cm^{-1} from absorbed water and surface oxides, as well as the C=O vibration of carboxyl groups at ~ 1713 cm^{-1} [43]. The presence of oxygen-containing groups made ATCNTs to be negatively charged in ethanol. Correspondingly, the zeta potential of ATCNT colloid was determined as -39.5 mV; this prevented the individual dispersed ATCNTs from aggregating, therefore maintaining a stable colloid.

To better understand the effect of ATCNT addition on the powder mixing, typical suspensions of 10% Al_2O_3 /MoTiAl and 10% Al_2O_3 -0.31%ATCNT/MoTiAl mixture were statically left for a period. As shown in Fig. 3a, obvious stratification is observed for the Al_2O_3 /MoTiAl colloid. The Al_2O_3 nanoparticles were mutually repulsive and remained a stable dispersion in the supernatant even after 2 h, while MoTiAl powders quickly sedimented at the bottom of the beaker under gravity. Interestingly, such stratification was not detected in the Al_2O_3 -ATCNT/MoTiAl mixture; the supernatant became transparent after settling for a brief time of 0.15 h (Fig. 3b). It indicates that the ATCNTs may play a role in bridging the Al_2O_3 and MoTiAl powders.

Fig. 4 shows the morphologies of composite powders via FESEM. The uniform dispersion of Al_2O_3 (see white granule phases in Fig. 4a) was observed in a 5% Al_2O_3 -0.15%ATCNT/MoTiAl powder. Al_2O_3 nanoparticles are tightly and sparingly covering the surface of MoTiAl so that

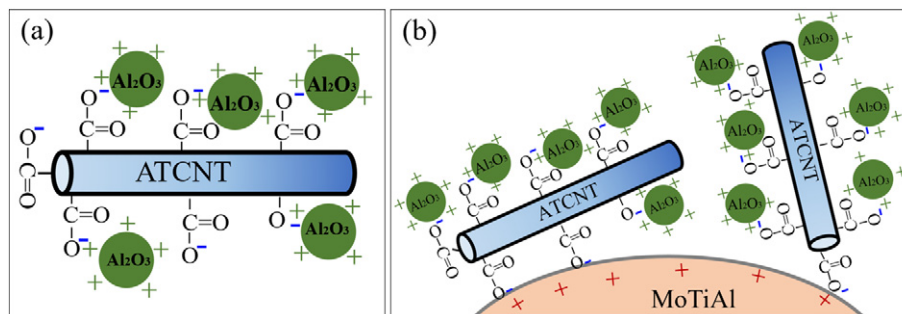


Fig. 5. Schematic illustration of the developed strategy for preparing Al_2O_3 -ATCNT/MoTiAl composite powders.

the MoTiAl powders remain in their original states [e.g., similar shape (see Fig. 4b), particle size and distribution (see Table 2)]. In other words, the features of composite powders seem to be controllable, merely depending on the features of the starting metallic powders rather than the fabrication processes (e.g., HEBM). No obvious aggregation of Al_2O_3 was present up to a high concentration of 10% (Fig. 4c). Instead, the increased surface area of MoTiAl was wrapped with Al_2O_3 nanoparticles (Fig. 4d). Few Al_2O_3 clusters were detected beyond 10% (Fig. S3, Supporting information). That is mainly attributed to the limited contact surface of MoTiAl as compared to the total surface area of Al_2O_3 nanoparticles during powder mixing.

Magnified FESEM images showed the existence of ATCNTs (see black arrows in Fig. 4e and f). The critical role played by ATCNTs in bridging the Al_2O_3 and MoTiAl powders as predicted is exactly clarified. Fig. 4e shows several Al_2O_3 nanoparticles coating the surface of an ATCNT, one tip of which is intimately bonded to a MoTiAl powder. Fig. 4f displays two ATCNTs partially wrapped with Al_2O_3 lying on the surface of the MoTiAl powder.

Based on the microstructural observations, the fabrication strategy for Al_2O_3 -ATCNT/MoTiAl powders could be simply understood as follows. Firstly, the ATCNTs were partially covered with Al_2O_3 nanoparticles by electrostatic self-assembly in a 3% ATCNT/ Al_2O_3 powder

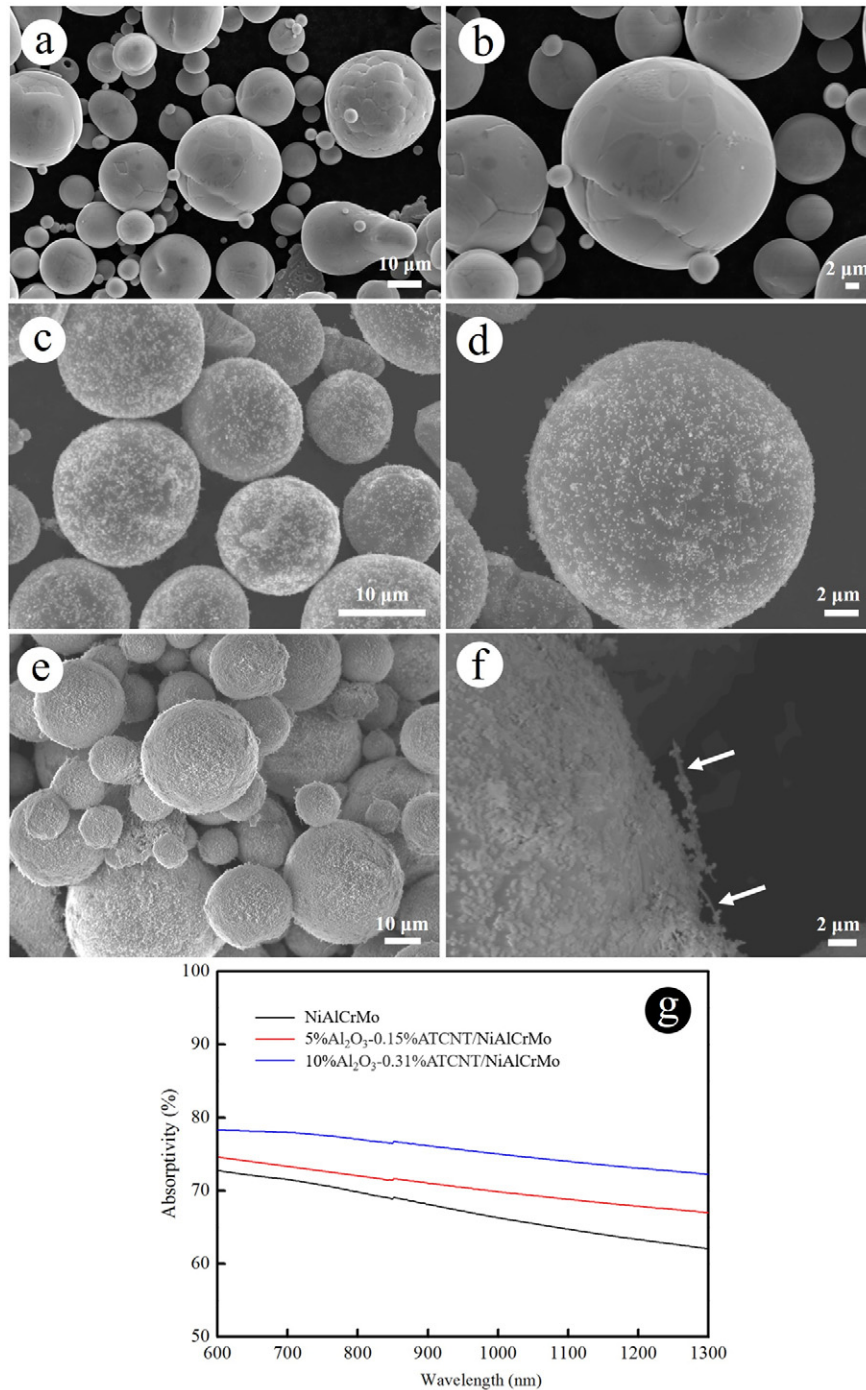


Fig. 6. FESEM images of (a, b) raw NiAlCrMo, (c, d) 5% Al_2O_3 -0.15% ATCNT/NiAlCrMo and (e, f) 10% Al_2O_3 -0.31% ATCNT/NiAlCrMo powders; (g) Laser absorptivity of NiAlCrMo, 5% Al_2O_3 -0.15% ATCNT/NiAlCrMo, and 10% Al_2O_3 -0.31% ATCNT/NiAlCrMo powders as a function of laser wavelength in a range of 600–1300 nm. The white arrows in (f) show two individual ATCNTs which are partially covered with Al_2O_3 nanoparticles.

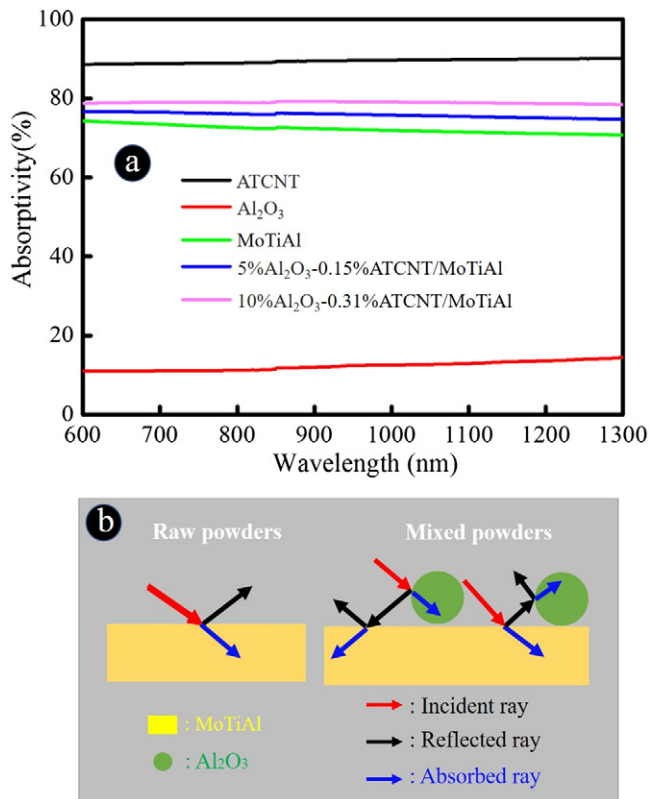


Fig. 7. (a) Laser absorptivity of ATCNTs, Al₂O₃, MoTiAl, 5%Al₂O₃-0.15%ATCNT/MoTiAl, and 10%Al₂O₃-0.31%ATCNT/MoTiAl powders as a function of laser wavelength in a range of 600–1300 nm; (b) schematic illustration revealing the difference in laser absorptivity between raw MoTiAl and Al₂O₃-ATCNT/MoTiAl mixed powders.

(Fig. 5a). The distance between two adjacent Al₂O₃ nanoparticles on one ATCNT was determined to be ~50–800 nm (Fig. 4e and f). Mehdi et al. [45] recently synthesized various ATCNT/Al₂O₃ mixtures by using the same starting materials as used in this work. They realized that the entire surface of an individual ATCNT was just wrapped with Al₂O₃ nanoparticles at an ATCNT concentration of 1.3%. Thanks to the ~70 mV attractive potential between ATCNTs and Al₂O₃ nanoparticles, the ATCNT-Al₂O₃ interfacial bonding was strong and irreversible [45]. Subsequently, the uncovered surface areas of ATCNTs allow them to be intimately bonded to the positively charged MoTiAl (Fig. 5b), which realized the homogeneous adsorption of Al₂O₃ nanoparticles on MoTiAl powders.

To further validate the feasibility of this strategy for nanoceramic/metal powders, spherical NiAlCrMo powders with a mean particle size of 27.1 μm were also combined with Al₂O₃ nanoparticles. The experimental conditions were the same as those for Al₂O₃-ATCNT/MoTiAl powders. Interestingly, a similar result was obtained; that is, individual Al₂O₃ nanoparticles were intimately wrapped on the surface of NiAlCrMo powders, thanks to the bridging effect of ATCNTs (Fig. 6f). Accordingly, it can be concluded that using ATCNTs as an agent during heteroagglomeration is a facile and effective approach to fabricating uniform nanoceramic/metal composite powders that maintain a similar shape, particle size, and distribution as those of the original metallic powders.

In addition to morphology and flowability, the laser absorptivity of powders is a key factor for influencing PBF processability. It directly determines how much power the powders absorb at a certain laser wavelength, λ, to form a melt. Fig. 7a shows the laser absorptivity of different powders as a function of λ. At λ = 1070 nm (the wavelength used in this work), the laser absorptivity of ATCNT or MoTiAl is approximately 89.8% or 71.6%, respectively; in contrast, Al₂O₃ possesses a significantly lower value of 12.8%. Since only small quantities of ATCNTs (~0.3%) were incorporated and their surfaces were partially coated with Al₂O₃ nanoparticles, the effect of ATCNTs on the laser absorptivity of composite powders was minute (Fig. S4, Supporting information).

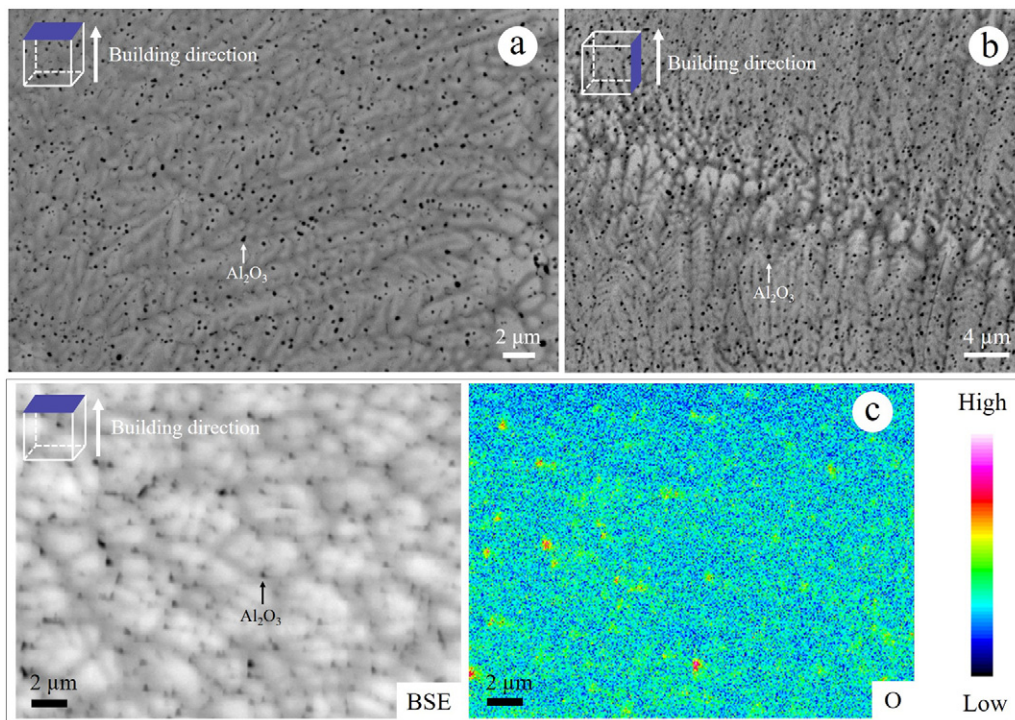


Fig. 8. FESEM-BSE images of (a) the transversal and (b) longitudinal cross-section of a PBF-processed 5%Al₂O₃-0.15%ATCNT/MoTiAl composite; (c) BSE image and EPMA mapping of elemental O for the transversal cross-section of 5%Al₂O₃-0.15%ATCNT/MoTiAl composite.

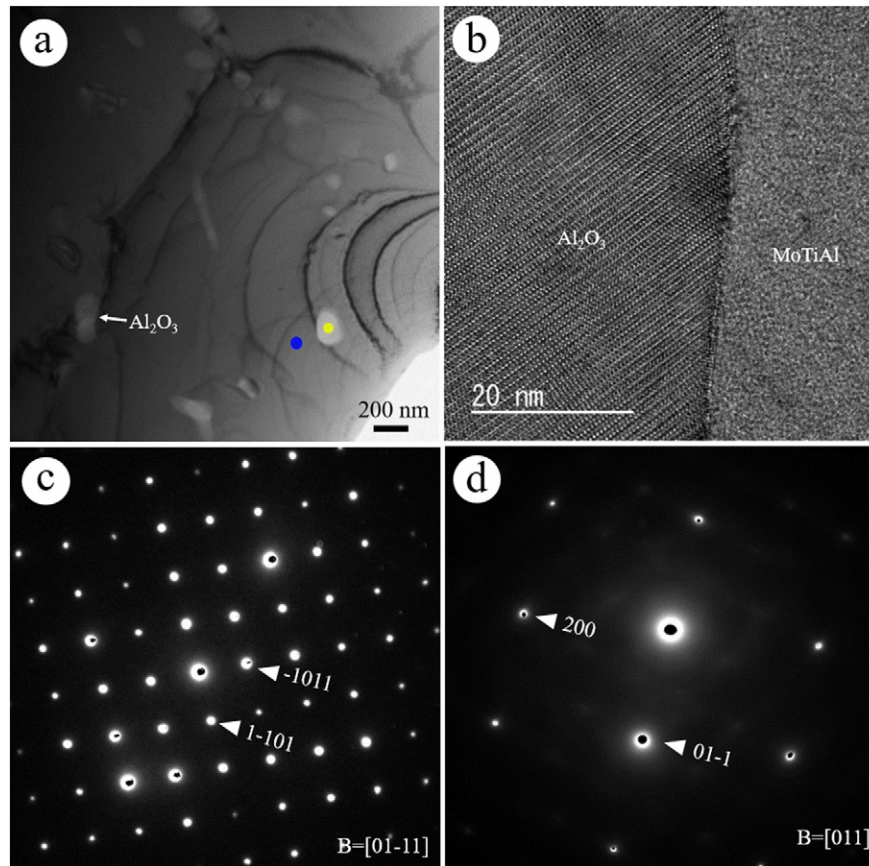


Fig. 9. (a, b) Bright-field TEM images showing the transversal cross-section of a PBF-processed 5%Al₂O₃-0.15%ATCNT/MoTiAl composite; (c, d) SAED patterns of Al₂O₃ and MoTiAl taken from yellow and blue spots in (a), respectively.

According to the mixing principle suggested by Tolochko et al. [46], the laser absorptivity of mixtures, A , is given by:

$$A = A_1\gamma_1 + A_2\gamma_2,$$

where A_i and γ_i are the laser absorptivity and concentration of component i , respectively. It seems that Al₂O₃ is incorporated to reduce the absorptivity of MoTiAl powders. However, the absorptivity of 5%Al₂O₃-0.15%ATCNT/MoTiAl and 10%Al₂O₃-0.31%ATCNT/MoTiAl powders was determined to increase by 5.5% and 10.3%, respectively (Fig. 7a). This striking result is possibly due to an increased surface roughness of Al₂O₃-coated MoTiAl [47]. As illustrated in Fig. 7b, a portion of an incident ray reflects specularly from the surface, which has no further interaction with raw MoTiAl. However, for Al₂O₃-ATCNT/MoTiAl powders, the protruded Al₂O₃ nanoparticles on the MoTiAl surface benefit multiple absorptions of laser radiation. In addition, surface unevenness usually causes absorption events at high angles of incidence (close to the Brewster angle), contributing to higher local laser absorptivity [47]. The Al₂O₃-coated MoTiAl or NiAlCrMo powders (see Fig. 6g) with high laser absorptivity are expected to improve PBF processability. This result may provide new insights for processing refractory intermetallics by PBF.

In order to fully prove the suitability for additive manufacturing, the composite powders were processed by laser PBF. Fig. 8 shows the FESEM-backscattered electron (BSE) images of a PBF-processed 5%Al₂O₃-0.15%ATCNT/MoTiAl composite. A dense composite was obtained. No unmelted metallic particles or micropores were observed in this composite. The EPMA mapping (Fig. 8c) and SEM-EDS analysis (Fig. S5, Supporting information) reveal that the black spots in Fig. 8a and b consist of elemental O and Al, which should correspond to Al₂O₃. It seems that a slight increase in the surface roughness of Al₂O₃-coated MoTiAl has limited deterioration for powder flowability during PBF. A fine dendrite structure was observed in the composite, possibly

attributing to the superfast cooling speed of laser PBF ($\sim 10^3$ – 10^8 Ks⁻¹ [48]) and the incorporation of Al₂O₃ that promotes heterogeneous nucleation during solidification.

Further analysis was performed by TEM. As revealed by the corresponding selected area electron diffraction (SAED) patterns in Fig. 9c and d, the white granule phases marked by the arrow in Fig. 9a (i.e., the black spots in Fig. 8) are the Al₂O₃, while the residual zone corresponds to the MoTiAl matrix. It is clearly seen that the Al₂O₃ nanoparticles are well dispersed and homogeneously distributed in the

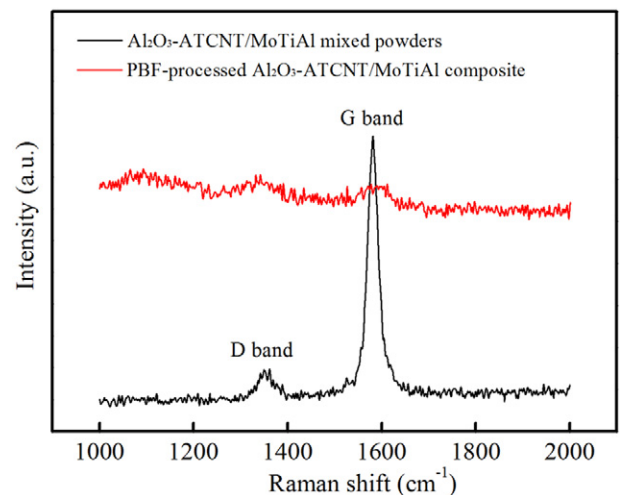


Fig. 10. Raman spectra of Al₂O₃-ATCNT/MoTiAl mixed powders and PBF-processed Al₂O₃-ATCNT/MoTiAl composite.

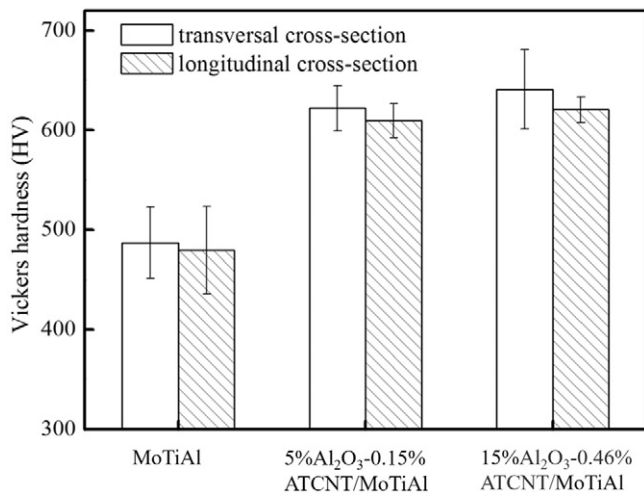


Fig. 11. Vickers hardnesses of PBF-processed pure MoTiAl and 15%Al₂O₃-0.46%ATCNT/MoTiAl composites in the transversal and longitudinal cross-sections, respectively.

composite. This is possibly attributed to (i) the preparation of uniform Al₂O₃-ATCNT/MoTiAl powders and (ii) the Marangoni convention and resultant capillary forces for liquid flow induced during the PBF process, which could promote the homogeneity of Al₂O₃ [49]. The distance between two adjacent Al₂O₃ nanoparticles ranges from 50 nm to 1 μm (Fig. 9a), which is similar to that of two adjacent Al₂O₃ particles on an ATCNT (Fig. 4e and f). Fig. 9b shows that the Al₂O₃/MoTiAl interface is very clean, which is highly free of interfacial impurities. Since there is insignificant discrepancy in thermal expansion coefficients between the Al₂O₃ ($\sim 5.4 \times 10^{-6} \text{ K}^{-1}$ [50]) and Mo ($\sim 4.8 \times 10^{-6} \text{ K}^{-1}$ [51]), no microcrack was detected at this Al₂O₃/MoTiAl interface during solidification, showing good interfacial compatibility.

Considering the sensitivity of XRD analysis, Micro-Raman spectroscopy, as a very powerful tool for sensing sp² carbon correlating materials, was performed to determine the evolution of ATCNTs during PBF. As revealed in Fig. 10, the Al₂O₃-ATCNT/MoTiAl mixed powders have two characteristic peaks: the D peak at 1350 cm⁻¹ is associated with the presence of lattice disorders, while the G band at 1580 cm⁻¹ strongly corresponds to in-plane C—C symmetric stretching vibrations in graphene sheets. However, those key features of ATCNTs were not identified in the PBF-processed Al₂O₃-ATCNT/MoTiAl composites. Careful TEM observations also confirmed that the ATCNTs were not retained after PBF. Two possible reasons were responsible for this phenomenon. One is the decomposition of ATCNTs. As mentioned above, the ATCNTs possessing higher absorptivity would absorb more laser energy and was likely to be heated to a higher temperature than the surrounding MoTiAl matrix, facilitating the dissolution of ATCNT structures in the MoTiAl melting pools [14]. The other is that the ATCNTs were reacted with the matrix [52], since abundant dangling bonds of carbon atoms existed in the ATCNTs (see Fig. 2f and g).

Fig. 11 shows the Vickers hardnesses of PBF-processed pure MoTiAl and Al₂O₃-ATCNT/MoTiAl composite. The Vickers hardnesses of pure MoTiAl were measured as 487.2 and 479.7 in the transversal and longitudinal cross-sections, respectively. The Vickers hardnesses of the 5%Al₂O₃-0.15%ATCNT/MoTiAl composite were 622.1 and 609.6 in the transversal and longitudinal cross-sections. The enhancement of Vickers hardnesses should be predominantly attributed to the well-dispersed Al₂O₃ nanoparticles, which had the load-bearing capability to suppress the dislocation motion and plastic deformation of MoTiAl matrix. However, As the Al₂O₃ concentration increased to 15%, the composite hardness did not further increase due to the aggregation of Al₂O₃ (Fig. S6, Supporting information). Very recently, Ma et al. [30] reported that the addition of nanoparticles could increase the melted zone depth while shrinking the size of the heat-affected zone so as to influence

the properties of PBF-processed MMCs. Thus, the influence of Al₂O₃ nanoparticles on the microstructures and mechanical performance of Al₂O₃-ATCNT/MoTiAl composites (e.g., elevated-temperature strength) should be systemically evaluated in future work.

4. Conclusions

In summary, we have successfully developed a novel strategy to fabricate Al₂O₃-nanoparticle/metal composite powders for PBF by using ATCNTs as an agent during heteroagglomeration. The negatively charged ATCNTs effectively bridged positively charged Al₂O₃ and MoTiAl powders utilizing electrostatic attraction. It made individual Al₂O₃ nanoparticles uniformly coat the surface of MoTiAl without aggregation of up to 10%. The Al₂O₃-coated MoTiAl powders maintained a shape, particle size, and distribution similar to those of uncoated ones. Simultaneously, their laser absorptivity was largely improved due to an increased surface roughness for multiple absorptions of laser radiation. In addition, a similar result was obtained in Al₂O₃-ATCNT/NiAlCrMo system; that is, individual Al₂O₃ nanoparticles were tightly wrapped on the surface of NiAlCrMo powders, thanks to the bridging effect of ATCNTs.

The PBF-processed Al₂O₃-ATCNT/MoTiAl composite was proved to be dense, in which Al₂O₃ nanoparticles were homogeneously dispersed and intimately contacted with the matrix. No ATCNT structure was retained after PBF might due to the decomposition and/or chemical reactions. It is confirmed that the Vickers hardness of MoTiAl matrix was exactly increased with incorporation of Al₂O₃ nanoparticles. Our finding may offer significant guidance for designing and producing advanced Mo-based composites in the application of heat-resistant materials.

Acknowledgment

This work was partially supported by the New Energy and Industrial Technology Department Organization (NEDO) in Japan through the Energy and Environment New Technology Leading Program (No. 14102987-0). The authors would like to thank Dr. Takamichi Miyazaki and Dr. Kosei Kobayashi for their sophisticated skill in TEM.

Appendix A. Supplementary data

Supplementary data to this article can be found online at <https://doi.org/10.1016/j.matdes.2017.10.034>.

References

- [1] S.M. Zebarjad, S.A. Sajjadi, Dependency of physical and mechanical properties of mechanical alloyed Al–Al₂O₃ composite on milling time, *Mater. Design* 28 (2007) 2113–2120.
- [2] I.A. Ibrahim, F.A. Mohamed, E.J. Lavernia, Particulate reinforced metal matrix composites - a review, *J. Mater. Sci.* 26 (1991) 1137–1156.
- [3] M.K. Surappa, Aluminium matrix composites: challenges and opportunities, *Sadhana* 28 (2003) 319–334.
- [4] K. Yoshimi, J. Nakamura, D. Kanekon, S. Yamamoto, K. Maruyama, H. Katsui, et al., High-temperature compressive properties of TiC-added Mo–Si–B alloys, *JOM* 66 (2014) 1930–1938.
- [5] W. Zhou, T. Yamaguchi, K. Kikuchi, N. Nomura, A. Kawasaki, Effectively enhanced load transfer by interfacial reactions in multi-walled carbon nanotube reinforced Al matrix composites, *Acta Mater.* 125 (2017) 369–376.
- [6] H. Chen, Q. Ma, X. Shao, J. Ma, C. Wang, B. Huang, Microstructure, mechanical properties and oxidation resistance of Mo₅Si₃–Al₂O₃ composite, *Mat. Sci. Eng. A-Struc.* 592 (2014) 12–18.
- [7] M. Krasnowski, T. Kulik, Nanocomposites obtained by mechanical alloying in Fe–Al–Ti–C system, *J. Alloys Compd.* 448 (2008) 227–233.
- [8] H. Arami, A. Simchi, Reactive milling synthesis of nanocrystalline Al–Cu/Al₂O₃ nanocomposite, *Mat. Sci. Eng. A-Struc.* 464 (2007) 225–232.
- [9] S.C. Tjong, Novel nanoparticle-reinforced metal matrix composites with enhanced mechanical properties, *Adv. Eng. Mater.* 9 (2007) 639–652.
- [10] T. Rong, D.D. Gu, Formation of novel graded interface and its function on mechanical properties of WC_{1-x} reinforced Inconel 718 composites processed by selective laser melting, *J. Alloys Compd.* 680 (2016) 333–342.

- [11] D.D. Gu, W. Meiners, K. Wissenbach, R. Poprawe, Laser additive manufacturing of metallic components: materials, processes and mechanisms, *Int. Mater. Rev.* 57 (2012) 133–164.
- [12] J.P. Kruth, L. Froyen, J. Van Vaerenbergh, P. Mercelis, M. Rombouts, B. Lauwers, Selective laser melting of iron-based powder, *J. Mater. Process. Technol.* 149 (2004) 616–622.
- [13] F. Abe, K. Osakada, M. Shiomi, K. Uematsu, M. Matsumoto, The manufacturing of hard tools from metallic powders by selective laser melting, *J. Mater. Process. Technol.* 111 (2001) 210–213.
- [14] L. Thijs, F. Verhaeghe, T. Craeghs, J.V. Humbeeck, J.-P. Kruth, A study of the microstructural evolution during selective laser melting of Ti–6Al–4V, *Acta Mater.* 58 (2010) 3303–3312.
- [15] T. Rong, D. Gu, Q. Shi, S. Cao, M. Xia, Effects of tailored gradient interface on wear properties of WC/Inconel 718 composites using selective laser melting, *Surf. Coat. Technol.* 307 (2016) 418–427.
- [16] D.D. Gu, Z.Y. Wang, Y.F. Shen, Q. Li, Y.F. Li, In-situ TiC particle reinforced Ti–Al matrix composites: powder preparation by mechanical alloying and selective laser melting behavior, *Appl. Surf. Sci.* 255 (2009) 9230–9240.
- [17] B. Song, S.J. Dong, C. Coddet, Rapid in situ fabrication of Fe/SiC bulk nanocomposites by selective laser melting directly from a mixed powder of micro-sized Fe and SiC, *Scr. Mater.* 75 (2014) 90–93.
- [18] D.D. Gu, H.Q. Wang, D.H. Dai, P.P. Yuan, W. Meiners, R. Poprawe, Rapid fabrication of Al-based bulk-form nanocomposites with novel reinforcement and enhanced performance by selective laser melting, *Scr. Mater.* 96 (2015) 25–28.
- [19] X.P. Li, G. Ji, Z. Chen, A. Addad, Y. Wu, H.W. Wang, et al., Selective laser melting of nano-TiB₂ decorated AlSi10Mg alloy with high fracture strength and ductility, *Acta Mater.* 129 (2017) 183–193.
- [20] B. Zhang, G. Bi, S. Nai, C.-N. Sun, J. Wei, Microhardness and microstructure evolution of TiB₂ reinforced Inconel 625/TiB₂ composite produced by selective laser melting, *Opt. Laser Technol.* 80 (2016) 186–195.
- [21] Q.Q. Han, R. Setchi, S.L. Evans, Synthesis and characterisation of advanced ball-milled Al–Al₂O₃ nanocomposites for selective laser melting, *Powder Technol.* 297 (2016) 183–192.
- [22] J.B. Jue, D.D. Gu, K. Chang, D.H. Dai, Microstructure evolution and mechanical properties of Al–Al₂O₃ composites fabricated by selective laser melting, *Powder Technol.* 310 (2017) 80–91.
- [23] D.D. Gu, G.B. Meng, C. Li, W. Meiners, R. Poprawe, Selective laser melting of TiC/Ti bulk nanocomposites: influence of nanoscale reinforcement, *Scr. Mater.* 67 (2012) 185–188.
- [24] H. Attar, M. Bonisch, M. Calin, L.C. Zhang, S. Scudino, J. Eckert, Selective laser melting of in situ titanium–titanium boride composites: processing, microstructure and mechanical properties, *Acta Mater.* 76 (2014) 13–22.
- [25] X.P. Li, C. Kong, T. Becker, T. Sercombe, Investigation of interfacial reaction products and stress distribution in selective laser melted Al12Si/SiC composite using confocal Raman microscopy, *Adv. Eng. Mater.* 18 (2016) 1337–1341.
- [26] H. Attar, S. Ehtemam-Haghighi, D. Kent, I.V. Okulov, H. Wendrock, M. Bonisch, M. Nanoindentation and wear properties of Ti and Ti–TiB composite materials produced by selective laser melting, *Mat. Sci. Eng. A-Struc.* 688 (2017) 20–26.
- [27] W. Li, W. Y. Yang, J. Liu, Y. Zhou, M. Li, S.F. Wen, enhanced nanohardness and new insights into texture evolution and phase transformation of TiAl/TiB₂ in-situ metal matrix composites prepared via selective laser melting, *Acta Mater.* 136 (2017) 90–104.
- [28] B. AlMangour, D. Grzesiak, M. Jenn, Selective laser melting of TiC reinforced 316L stainless steel matrix nanocomposites: influence of starting TiC particle size and volume content, *Mater. Design* 104 (2016) 141–151.
- [29] J.B. Jue, D.D. Gu, Selective, Laser melting additive manufacturing of in situ Al₂Si₄O₁₀/Al composites: microstructural characteristics and mechanical properties, *J. Compos. Mater.* 51 (2017) 519–532.
- [30] C. Ma, L.Y. Chen, C.Z. Cao, X.C. Li, Nanoparticle-induced unusual melting and solidification behaviours of metals, *Nat. Commun.* 8 8 (2017) 1–7.
- [31] T.A. Parthasarathy, M.G. Mendiratta, D.M. Dimiduk, Oxidation mechanisms in Mo-reinforced Mo₅SiB₂(T–2)–Mo₃Si alloys, *Acta Mater.* 50 (2002) 1857–1868.
- [32] D.M. Dimiduk, J.H. Perepezko, Mo–Si–B alloys: developing a revolutionary turbine-engine material, *MRS Bull.* 28 (2003) 639–645.
- [33] G. Liu, G.J. Zhang, F. Jiang, X.D. Ding, Y.J. Sun, J. Sun, et al., Nanostructured high-strength molybdenum alloys with unprecedented tensile ductility, *Nat. Mater.* 12 (2013) 344–350.
- [34] J.H. Perepezko, The hotter the engine, the better, *Science* 326 (2009) 1068–1069.
- [35] F. Baras, D.K. Kondepudi, F. Bernard, Combustion synthesis of MoSi₂ and MoSi₂–Mo₅Si₃ composites: multilayer modeling and control of the microstructure, *J. Alloys Compd.* 505 (2010) 43–53.
- [36] M. Parchovianský, D. Galusek, J. Sedláček, P. Švančárek, M. Kašiarová, J. Dusza, et al., Microstructure and mechanical properties of hot pressed Al₂O₃/SiC nanocomposites, *J. Eur. Ceram. Soc.* 33 (2013) 2291–2298.
- [37] B.B. He, K. Chang, W.H. Wu, C.L. Zhang, The formation mechanism of TiC reinforcement and improved tensile strength in additive manufactured Ti matrix nanocomposite, *Vacuum* 143 (2017) 23–27.
- [38] E.O. Olakanmi, R.F. Cochrane, K.W. Dalgarno, A review on selective laser sintering/melting (SLS/SLM) of aluminium alloy powders: processing, microstructure, and properties, *Prog. Mater. Sci.* 74 (2015) 401–477.
- [39] K. Rezwan, L.P. Meier, M. Rezwan, J. Voros, M. Textor, L.J. Gauckler, Bovine serum albumin adsorption onto colloidal Al₂O₃ particles: a new model based on zeta potential and UV-Vis measurements, *Langmuir* 20 (2004) 10055–10061.
- [40] M.D. Butterworth, R. Corradi, J. Johal, S.F. Lascelles, S. Maeda, S.P. Armes, Zeta potential measurements on conducting polymer–inorganic oxide nanocomposite particles, *J. Colloid Interface Sci.* 174 (1995) 510–517.
- [41] Y.C. Fan, G. Igarashi, W. Jiang, L.J. Wang, A. Kawasaki, Highly strain tolerant and tough ceramic composite by incorporation of graphene, *Carbon* 90 (2015) 274–283.
- [42] V.N. Popov, Carbon nanotubes: properties and application, *Mater. Sci. Eng. R* 43 (2004) 61–102.
- [43] W.W. Zhou, S. Sasaki, A. Kawasaki, Effective control of nanodefects in multiwalled carbon nanotubes by acid treatment, *Carbon* 78 (2014) 121–129.
- [44] Y.Y. Lu, J.P. Yamada, J. Nakamura, K. Yoshimi, H. Kato, Effect of B2-ordered phase on the deformation behavior of Ti–Mo–Al alloys at elevated temperature, *J. Alloys Compd.* 696 (2017) 130–135.
- [45] M. Estili, A. Kawasaki, An approach to mass-producing individually alumina-decorated multi-walled carbon nanotubes with optimized and controlled compositions, *Scr. Mater.* 58 (2008) 906–909.
- [46] N.K. Tolochko, T. Laoui, Y.V. Khlopkov, S.E. Mozzharov, V.I. Titov, M.B. Ignatiev, Absorbance of powder materials suitable for laser sintering, *Rapid Prototyp. J.* 6 (2000) 155–160.
- [47] L.K. Ang, Y.Y. Lau, R.M. Gilgenbach, H.L. Spindler, Analysis of laser absorption on a rough metal surface, *Appl. Phys. Lett.* 70 (1997) 696–698.
- [48] B. Vrancken, L. Thijs, J.-P. Kruth, J. Van Humbeeck, Heat treatment of Ti6Al4V produced by selective laser melting: microstructure and mechanical properties, *J. Alloys Compd.* 541 (2012) 177–185.
- [49] S. Dadbakhsh, L. Hao, Effect of Al alloys on selective laser melting behaviour and microstructure of in situ formed particle reinforced composites, *J. Alloys Compd.* 541 (2012) 328–334.
- [50] P. Auerkari, Mechanical and Physical Properties of Engineering Alumina Ceramics: Technical Research Centre of Finland Espoo, 1996.
- [51] F. Nix, D. MacNair, The thermal expansion of pure metals. II: molybdenum, palladium, silver, tantalum, tungsten, platinum, and lead, *Phys. Rev.* 61 (1942) 74.
- [52] X. Zhao, B. Song, W. Fan, Y. Zhang, Y. Shi, Selective laser melting of carbon/AlSi10Mg composites: microstructure, mechanical and electrical properties, *J. Alloys Compd.* 665 (2016) 271–281.